DOI: 10.21062/mft.2024.051 http://www.journalmt.com

Influence of Thermal-mechanical Coupling of Single Particle on Grinding Surface Roughness

Lai Hu (0000-0002-9660-9536), Zixi Wang (0009-0008-4704-2829)*, Yuming Wang (0000-0002-3918-2022).
State Key Laboratory of Tribology in Advanced Equipment, Tsinghua University, Beijing 100084, China.
*Condensing e-mail: zxwang@tsinghua.edu.cn

Grinding is one of the most important processes in machining precision rotating parts. GF & GT (grinding force and grinding temperature) of single particle in grinding wheel have great influence on surface roughness. In this study, the GF & GT models of single particle were established. Abaqus was used to analyze the coupling between GF & GT of single particle. Combined with grinding parameters (grinding depth and grinding speed), the influence of GF & GT on the range of surface roughness of single particle abrasive was comprehensively studied. The machining and experimental analysis of precision aerospace bearings were carried out through theoretical analysis. The results show that with the increase of grinding depth, the GF & GT in X and Z directions increase gradually. However, the grinding temperature does not increase linearly with the increase of grinding depth. Compared with the grinding speed, the influence of grinding depth on the grinding force in Y and Z directions is much greater than that in X, which is 7.38 times and 5.81 times of the grinding speed, respectively. Grinding depth has the greatest influence on surface roughness, which is 3.6 times of grinding speed. When the test speed is constant at 60000 rev/min, the bearing temperature is between 30 °C and 65 °C and most of them are within 44 °C. The test data meet the requirements, and all indexes are controllable. The above conclusions provide theoretical basis and selection of process optimization parameters for grinding precision rotating parts.

Keywords: GF & GT, Surface roughness, Single particle, Range analysis

1 Introduction

Grinding belongs to precision machining, which is generally used in the final process of precision parts [1]. The characteristics of grinding wheel are one of the guarantees of grinding quality [2]. In grinding wheel abrasive particles, the main components are single cutting abrasive particles and adhesive. In the grinding process, the essence is that a single abrasive particle forms a layer of effective cutting on the surface of the workpiece. The essence of grinding research is the research of single abrasive particle in the cutting process. GF & GT are the two most important parameters affecting surface roughness in grinding. And the control of GF & GT mainly comes from the control of grinding parameters. Therefore, this is a closed-loop study.

A series of scholars have made in-depth research on single particle grinding. For example, Lei et al. [3] carried out ultrasonic-assisted high-speed grinding experiment of single particle. A new dynamic grinding force model for ultrasonic-assisted high-speed grinding of single abrasive particles is established. Zhao et al. [4] proposed a new prediction model for single particle friction calculation, which is used to calculate ploughing friction coefficient with the aid of two-dimensional ultrasonic vibration (applying transverse vibration and additional normal vibration). Yan et al. [5] developed an improved cutting force model to analyze and evaluate the force-controlled robot abrasive belt grinding mechanism. The micro-scale of cutting force model composed of sliding, ploughing and cutting components was introduced. Krzysztof et al. [6] introduced a new method of mixing cooling and lubricating the processing area under dry conditions, taking the internal grinding of bearing rings as an example. The grinding ratio g is increased by more than 4 times by the proposed method. He et al. [7] reviewed the progress of the influence of grinding parameters on the surface of parts in ultra-precision machining of bearing rolling elements. Yao et al. [8] studied the GF & GT of ultra-high strength steel Aermet100 in conventional surface grinding with single alumina grinding wheel, white alumina grinding wheel and cubic boron nitride grinding wheel. When the grinding force is large and the grinding temperature is high, the workpiece material will adhere to a single alumina grinding wheel locally. Ding et al. [9] analyzed the contact pressure and load deformation of bearings by means of simulation, and proposed an innovative coordinated optimization method. References [10-12] are similar studies.

Based on the above research, there are few studies on the thermodynamic properties of single abrasive particles. In this study, the GF & GT model of single particle is established, and the GF & GT of single particle are simulated. The influence of grinding depth of single particle on GF & GT is analyzed, and the range of GF & GT on surface roughness is discussed. Finally, a comprehensive study is carried out through experiments.

2 Establishment of GF & GT model for single particle.

For the single-particle grinding state, the coupling model diagram of GF & GT was made, as shown in Fig. 1.

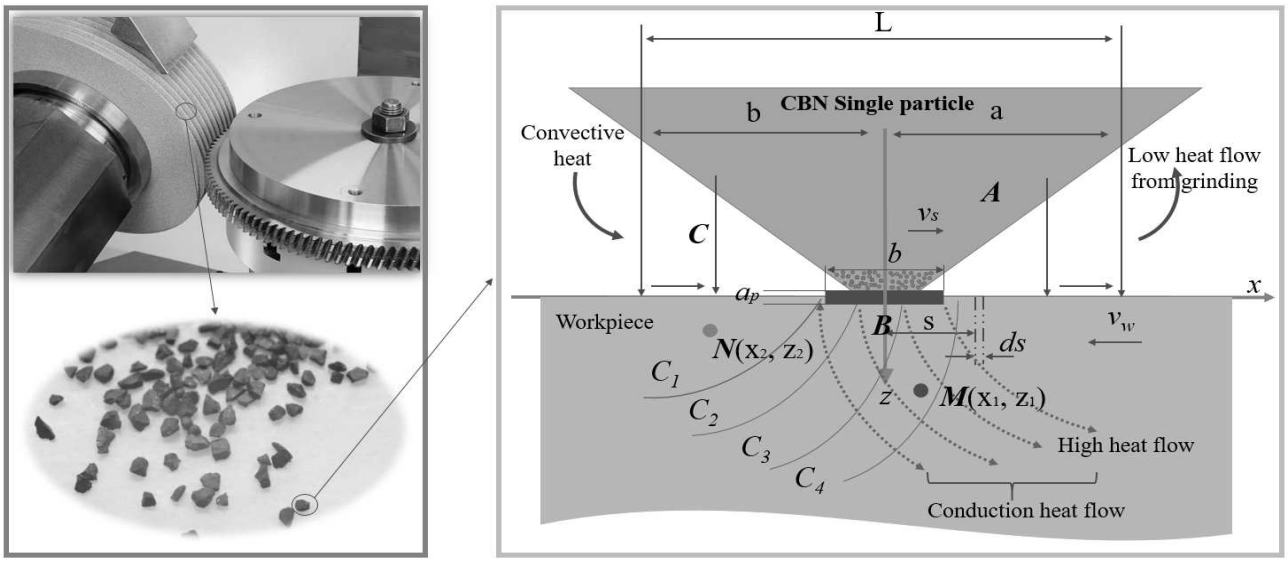

Fig. 1 *Model diagram of single particle GF & GT*

2.1 Single particle grinding force model

Grinding force of single particle is a main parameter to characterize grinding condition, and it is an important reason to generate grinding heat. Grinding force is an indispensable parameter in the calculation of grinding temperature. These formulas are expressed as power functions of grinding parameters, as shown in Eq. (1).

$$F_t = F_p a_p^{\alpha} v_s^{-\beta} v_w^{\gamma} b^{\delta} \tag{1}$$

Where:
F_t…Tangential grinding force;
F_p…Unit grinding force;
a_p…Grinding depth;
v_s…Wheel speed;
v_w…Workpiece speed;
b…Grinding width;
α, β, γ, δ…Exponents.

Due to the difference of grinding conditions and workpiece materials, the empirical Eqs. are also different. Since only three factors v_s, v_w and a_p are used in the experiment [13-14], the empirical formula of grinding force per unit width is Eq. (2).

$$F = C_F v_s^{b1} v_w^{b2} a_p^{b3} \tag{2}$$

Take logarithms on both sides of Eq. (2) and perform linear transformation to obtain Eq. (3):

$$\lg F = \lg C_F + b_1 \lg v_s + b_2 \lg v_w + b_3 \lg a_p \tag{3}$$

Where:
y=lgF;
$b_0=\lg C_F$;
x_1, x_2 and x_3…$\lg v_s$, $\lg v_w$ and $\lg v_p$ respectively, then Eq. (3) is transformed into Eq. (4):

$$y = b_0 + b_1 x_1 + b_2 x_2 + b_3 x_3 \tag{4}$$

By substituting 9 groups of experimental data in references [13-14] into Eq. (4), a set of equations is obtained Eq. (5):

$$y_i = b_0 + b_1 x_{i1} + b_2 x_{i2} + b_3 x_{i3} \tag{5}$$

i=1,2,….9

Introduce t vectors and matrix notations:

$$Y = \begin{bmatrix} y_1 \\ y_2 \\ \vdots \\ y_9 \end{bmatrix}, \quad X = \begin{bmatrix} 1\, x_{11}\, x_{12}\, x_{13} \\ 1\, x_{23}\, x_{23}\, x_{23} \\ \vdots\ \vdots\ \ \vdots\ \vdots \\ 1\, x_{91}\, x_{92}\, x_{93} \end{bmatrix}, \quad b = \begin{bmatrix} b_0 \\ b_1 \\ b_2 \\ b_3 \end{bmatrix}.$$

Then the regression model of Eq. (5) can be expressed in matrix form as Eq. (6):

$$Y=Xb \tag{6}$$

Where:

b_0, b_1, b_2 and b_3…Estimated by the least square method, and the Eq. (7) are obtained:

$$\hat{b}=(X^TX)^{-1}X^TY \tag{7}$$

Thus, the empirical Eq. (8) of grinding force per unit width are obtained:

$$\begin{cases} F_n^{'}=26.5v_s^{-0.641}v_w^{0.255}a_p^{0.718} \\ F_t^{'}=24.1v_s^{-0.848}v_w^{0.352}a_p^{0.705} \end{cases} \tag{8}$$

In order to introduce the equivalent single particle diameter de, the Eq. (8) is modified according to the relationship that the power exponent of grinding depth and the power exponent of equivalent single particle diameter in the theoretical equation of grinding force in reference [14-15] is 1, and finally the empirical equation. of grinding force per unit width Eq. (9) is obtained.

$$\begin{cases} F_n^{'}=5.95v_s^{-0.641}v_w^{0.255}a_p^{0.718}d_e^{0.282} \\ F_t^{'}=5.05v_s^{-0.848}v_w^{0.352}a_p^{0.705}d_e^{0.295} \end{cases} \tag{9}$$

Where:

$F'n$…Normal grinding force per unit width;

F'_t…Tangential grinding force per unit width;

d_e…Equivalent single particle diameter;

d_e=ds for surface grinding;

$d_e=d_sd_w/(d_w\pm d_s)$ for internal and external round grinding;

"+" for external round grinding;

"-" for internal round grinding;

d_s…Single particle diameter;

d_w…Workpiece diameter.

2.2 Temperature model of single particle grinding

According to Fig. 1 and the solid heat transfer theory [14-15], if the temperature rise $\theta_{z1=0}$ of any point M (x_1, 0) on the surface of AB zone is required, it can be calculated from the temperature field Eq. (10) of the continuous infinite surface heat source:

$$\theta_{z1=0}=\frac{q_m}{\lambda\sqrt{\pi}}\sqrt{4at} \qquad 0<x_1<l_{AB} \tag{10}$$

Where:

q_m…The heat flux flowing into the workpiece/$wm^{-2}s^{-1}$, calculated by Eq. (10).

λ…Materials thermal conductivity/$w.m^{-1}℃^{-1}$.

a…Thermal diffusivity of materials/$m^2\ s^{-1}$.

t…The time (s) the point is subjected to the surface heat source, $t=(L_{AB}-x_1)/v_{sl}$.

If the temperature rise θ_{z_1} of any point M (x_1, z_1) at different depths on the surface outside the AB region is required, it is calculated by the temperature field Eq. (11) of the continuous infinite surface heat source:

$$\theta_{z1}=\frac{q_m}{\lambda\sqrt{\pi}}z_1\Psi\left(\frac{z_1}{\sqrt{4at}}\right) \qquad 0<x_1<l_{AB} \tag{11}$$

Where:

$\Psi\left(\frac{z_1}{\sqrt{4at}}\right)$…Special function; $\Psi(p)=\int_p^{\infty}\frac{1}{u^2}e^{-u^2}du$.

If the temperature rise of any point N (x_2, 0) on the surface outside AB area is required, the workpiece material in the vertical direction where the point is located can be equivalent to a heat conduction rod. Obviously, the temperature of N (x_2, 0) is obtained from the instantaneous finite length surface heat source temperature calculation Eq. (12) after being continuously acted by surface heat source AB/v_{sl} time from point A and then cooled by BC/v_{sl} time. When the end face of the heat conduction body moves to point C, the temperature rise $\theta_{z_2=0}$ of N (x_2, 0) is obtained from the instantaneous finite length surface heat source temperature calculation Eq. (12):

$$\theta_{z_2}=\frac{q_m}{\lambda\sqrt{\pi}}\left[\sqrt{4at}-\sqrt{4a(t-\tau_0)}\right] \qquad x_2<0 \tag{12}$$

If the temperature rise θ_{z_2} of N (x_2, z_2) at any point of different depths below the surface outside AB region is required, Eq. (13) can be calculated from the instantaneous temperature field of finite surface heat source.

$$\theta_{z_2}=\frac{q_mz_2}{\lambda\sqrt{\pi}}\left\{\Psi\left[\frac{z_2}{\sqrt{4at}}\right]-\Psi\left[\frac{z_2}{\sqrt{4a(t-\tau_0)}}\right]\right\} \qquad x_2<0 \tag{13}$$

According to the solid one-dimensional heat conduction theory, the mathematical model of grinding temperature θ distribution in the workpiece grinding area is established as follows Eq. (14):

$$\theta_{(x,z)}=\begin{cases}\dfrac{q_m}{\lambda\sqrt{\pi}}\sqrt{4at} & 0<x<l_{AB},z=0\\ \dfrac{q_m}{\lambda\sqrt{\pi}}z\Psi\left(\dfrac{z}{\sqrt{4at}}\right) & 0<x<l_{AB},z>0\\ \dfrac{q_m}{\lambda\sqrt{\pi}}\left[\sqrt{4at}-\sqrt{4a(t-\tau_0)}\right] & x<0,z=0\\ \dfrac{q_m}{\lambda\sqrt{\pi}}\left\{\Psi\left[\dfrac{z}{\sqrt{4at}}\right]-\Psi\left[\dfrac{z}{\sqrt{4a(t-\tau_0)}}\right]\right\} & x<0,z>0\end{cases} \quad (14)$$

3 Simulation of GF & GT of single particle

3.1 Simulation modeling and mixed orthogonal design of single particle GF & GT

Carry out simulation modeling analysis according to Fig. 1, as shown in Fig. 2. Meanwhile, set CBN single particle and workpiece material parameters, as shown in Tab. 1 and Tab. 2. Mixed orthogonal experimental design was carried out for the simulation scheme, as shown in Tab 3.

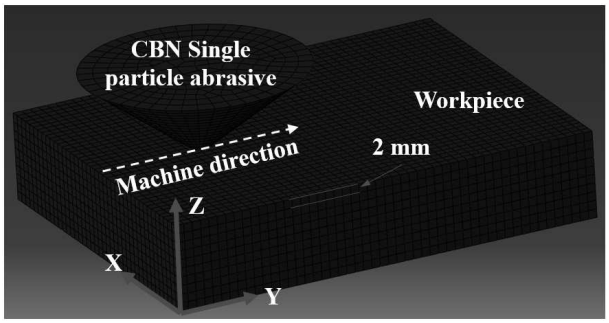

Fig. 2 *Simulation model*

Tab. 1 *CBN Single Particle Material Simulation Parameters*

Conductivity [w·m(-1)·k(-1)]	Density [Kg.m-3]	Poisson's ratio	Elastic modulus [GPa]	Coefficient of thermal expansion [K-1]	Specific heat [J/kg-1/°C-1]
42	3.5	0.24	720	2.1	670

Tab. 2 *Parameters of workpiece material simulation*

Temperature [°C]	Young's modulus [GPa]	Poisson's ratio	Coefficient of thermal expansion [K-1]	Conductivity [w·m-1·k-1]	Failure strain	Density [Kg/m3]	Specific heat [J/kg-1/°C-1]	Austenite phase change temperature [°C]
20	201	0.277	110.5	52.5	0.011	7812	458	750
200	179	0.269	12.6	47.5	0.070			
400	163	0.255	13.7	41.5	0.744			
600	103	0.342	13.7	32.5	2.542			
800	87	0.396	15.3	26.0	1.284			
1000	67	0.490	15.3	29.0	0.426			

Tab. 3 *Design of mixed orthogonal scheme for single particle grinding*

No.	Grinding speed [m.sec^{-1}]	Grinding depth [μm]	Grinding force F_x [N]	Grinding force F_y [N]	Grinding force F_z [N]	Grinding temperature [°C]	Ra [μm]
1	1(0.02)	1(1)	0.01	0.42	-1.21	10.15	0.43
2	3(0.04)	2(4)	0.01	1.7	-4.84	51.45	0.55
3	2(0.03)	3(8)	0.04	4.88	-9.64	102.08	1.1
4	3	4(12)	0.05	5.08	-14.43	149.06	2.09
5	2	5(16)	0.04	9.89	-19.85	196.92	2.36
6	1	6(20)	0.10	11.76	-23.75	166	1.96
7	2	7(30)	0.2	17.48	-36.78	356.56	4.2
8	1	8(40)	0.27	25.382	-48.34	317.83	5.56
9	3	9(50)	0.21	31.27	-56.57	528.81	4.85
10	1	9	0.22	31.266	-56.67	358.47	13.88
11	3	7	0.121	14.50	-35.79	369.42	4.63
12	2	8	0.58	24.97	-49.01	448.58	3.58
13	3	3	0.03	3.38	-9.65	100.19	1.44
14	2	1	0.01	0.47	-1.22	14.66	0.16
15	1	2	0.02	1.84	-4.78	34.31	0.58
16	2	6	0.11	12.9	-23.82	243.02	3.06
17	1	4	0.08	6.23	-14.22	103.42	1.44
18	3	5	0.06	7.34	-19.38	197.94	2.43
19	1	5	0.10	8.6	-19.4	135.76	1.73
20	3	6	0.08	9.78	-24.10	246.94	2.92
21	2	4	0.08	7.83	-14.38	150.77	1.76
22	3	8	0.15	25.71	-47.30	474.59	4.57
23	2	9	0.32	31.53	-59.90	476.18	6.21
24	1	7	0.25	19.44	-36.36	244.97	2.98
25	2	2	0.01	1.79	-4.83	52.56	0.56
26	1	3	0.06	4.24	-9.58	70.11	0.74
27	3	1	0.01	0.43	-1.22	16.41	0.17

As shown in Fig. 2, the grinding feed direction of CBN single particle model was Y direction, and the grinding depth feed direction is Z direction. According to the Hybrid Orthogonal Design Tab. 3, and for the convenience of subsequent block analysis, 27 sets of simulation results had been filled in, including X/Y/Z grinding force, grinding temperature and surface roughness in X/Y/Z direction.

3.2 Influence of grinding depth of single particle on GF & GT.

After processing 27 sets of simulation data in Tab. 3, the effects of grinding depth on X/Y/Z GF & GT at grinding speeds of 0.02 m.sec^{-1}, 0.03 m.sec^{-1} and 0.04 m.sec^{-1} were obtained, as shown in Figs. 3, 4 and 5, respectively.

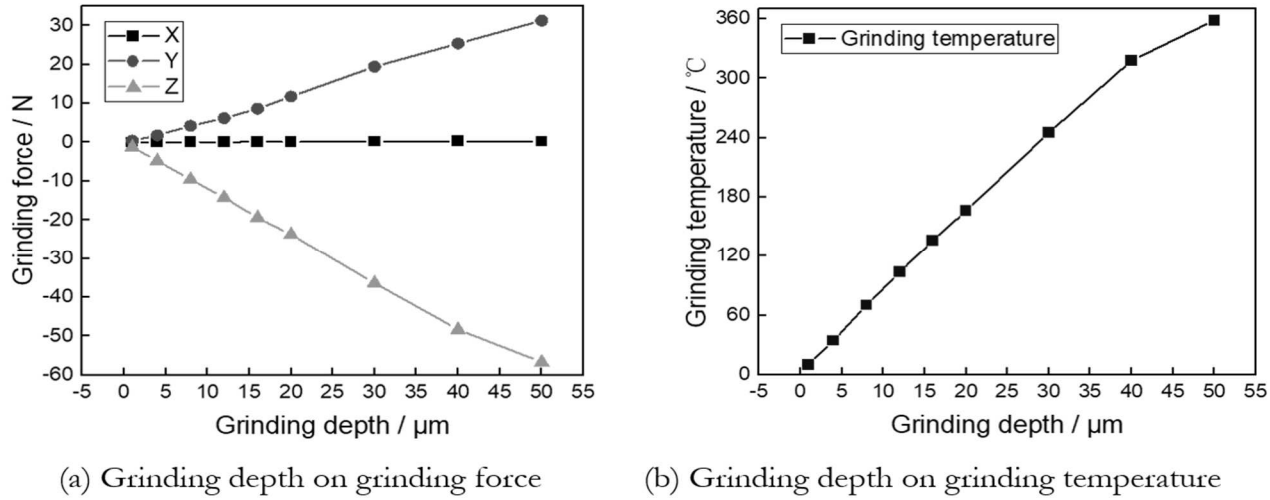

(a) Grinding depth on grinding force (b) Grinding depth on grinding temperature

Fig. 3 *Influence of grinding depth on GF & GT at grinding speed of 0.02 m.sec-1*

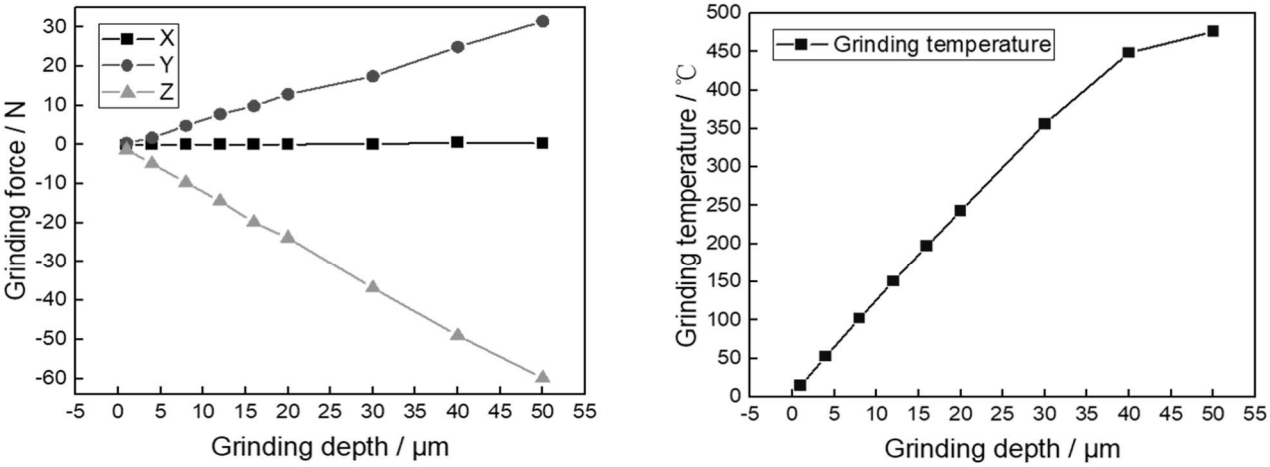

(a) Grinding depth on grinding force (b) Grinding depth on grinding temperature

Fig. 4 *Influence of grinding depth on GF & GT at grinding speed of 0.03 m.sec-1*

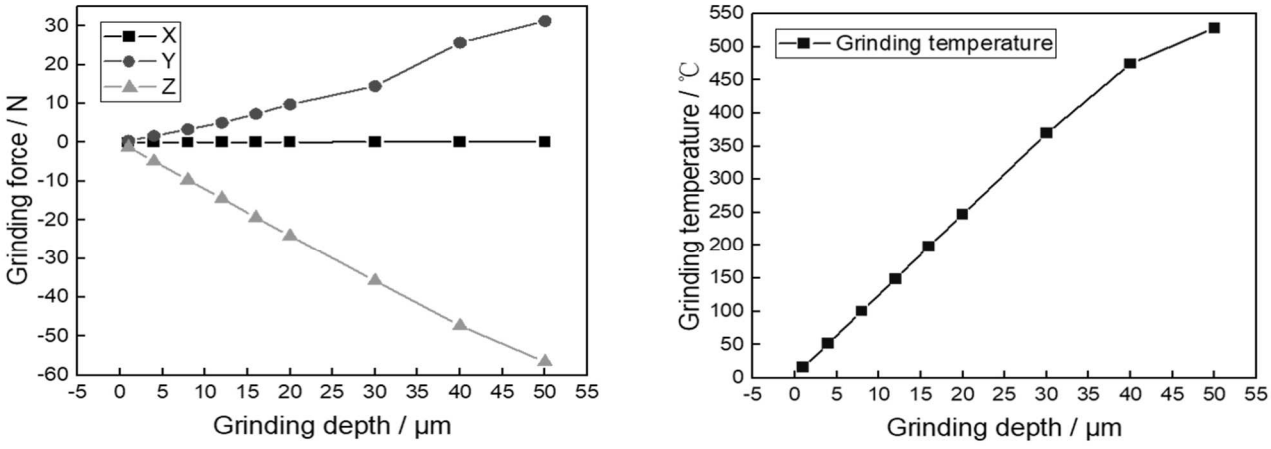

(a) Grinding depth on grinding force (b) Grinding depth on grinding temperature

Fig. 5 *Influence of grinding depth on GF & GT at grinding speed of 0.04 m.sec-1*

Macroscopic analysis of Figs. 3, 4 and 5 shown that the grinding force in Z direction was compressive stress, while that in X direction was tensile stress, and the grinding force in Z direction was always greater than that in X and Y directions. The grinding force in X direction was always 0 N. This conformed to

the X/Y/Z coordinate system of the simulation model in Fig. 2. With the increased of grinding depth, the GF & GT in X and Z directions gradually increased.

Microscopic analysis of Figs. 3, 4 and 5 shown that with the deepening of grinding depth, the grinding speed had almost no change on X/Y/Z grinding force. When the grinding speed was 0.02 m.sec^{-1}, 0.03 m.sec^{-1} and 0.04 m.sec^{-1} and the grinding depth is 50 μm, the grinding forces in X/Y/Z direction were 0 N, 31 N and 59 N, respectively. However, it was found that the grinding temperature increases not only with the increase of grinding depth, but also with the increase of grinding speed. When the grinding speed is 0.02 m.sec^{-1}, 0.03 m.sec^{-1} and 0.04 m.sec^{-1} and the grinding depth was 50 μm, the grinding temperature was 360 °C, 475 °C and 525 °C, respectively. When the grinding depth ranges from 1 μm to 40 μm, the grinding temperature increases linearly. When the grinding depth is 40 μm - 50 μm, the grinding temperature does not increase "rapidly", but becomes "slowly" relative to the grinding depth of 1 μm - 40 μm. It shown that the grinding temperature does not increase linearly with the increase of grinding depth, and at a certain time, the grinding temperature will change differently.

4 Surface roughness analysis of single particle grinding

4.1 Influence of single particle GF & GT on surface roughness

Surface roughness refers to the roughness of the machined surface with small spacing and tiny peaks and valleys. The distance between two peaks or troughs (wave distance) belongs to geometric error. The smaller the surface roughness, the smoother the surface. The effects of X/Y/Z GF & GT on grinding surface roughness at grinding speeds of 0.02 m.sec^{-1}, 0.03 m.sec^{-1} and 0.04 m.sec^{-1} were obtained by processing 27 sets of simulation data in Tab. 3, as shown in Figs. 6, 7 and 8, respectively.

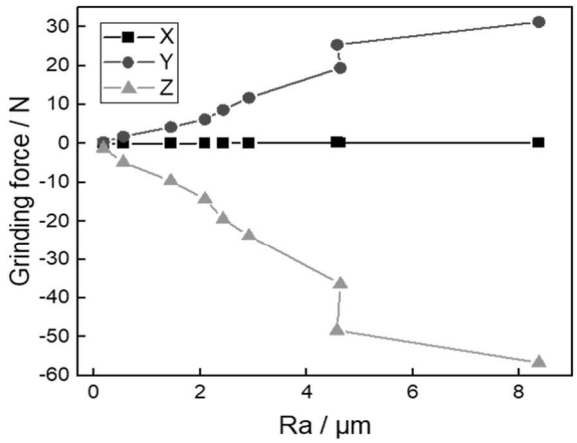

(a) Grinding force on surface roughness

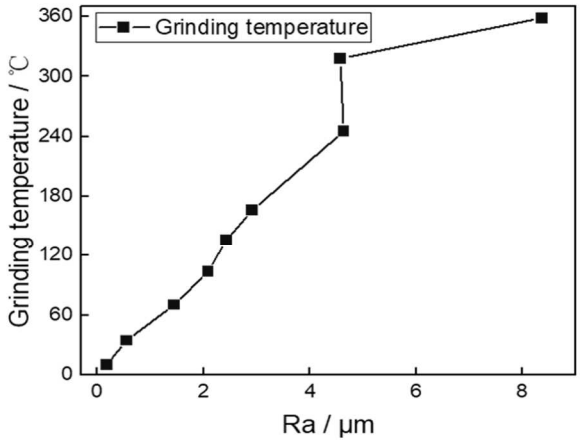

(b) Grinding temperature on surface roughness

Fig. 6 *Influence of GF & GT on surface roughness at grinding speed of 0.02 m.sec^{-1}*

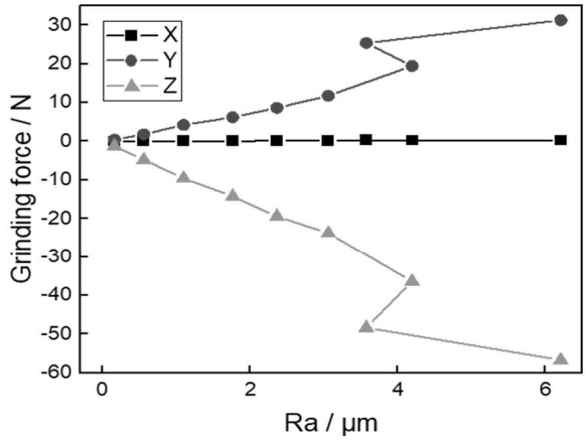

(a) Grinding force on surface roughness

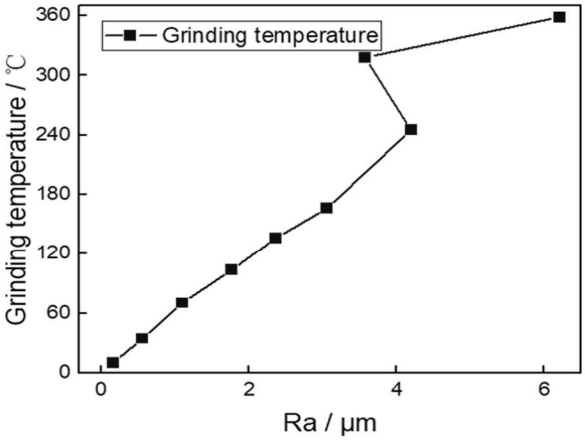

(b) Grinding temperature on surface roughness

Fig. 7 *Influence of GF & GT on surface roughness at grinding speed of 0.03 m.sec^{-1}*

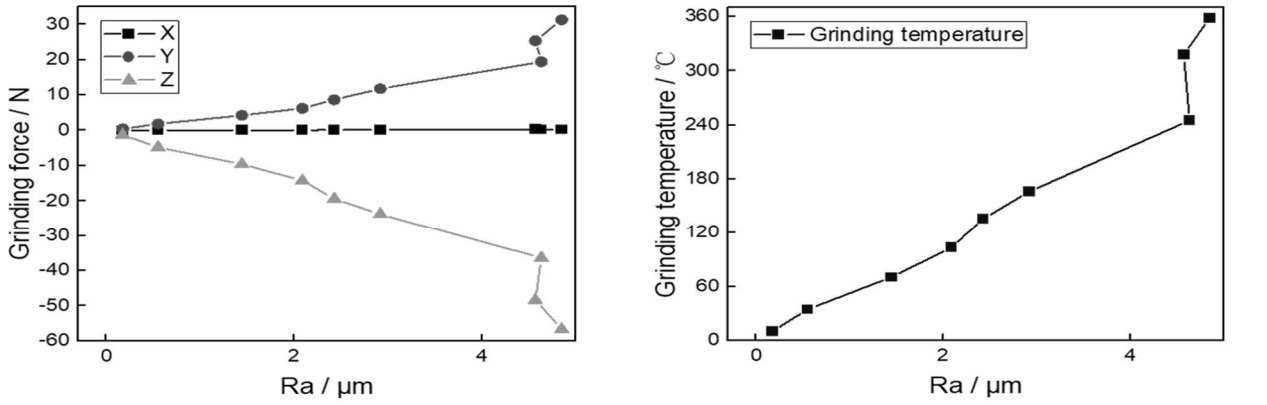

(a) Grinding force on surface roughness (b) Grinding temperature on surface roughness

Fig. 8 *Influence of GF & GT on surface roughness at grinding speed of 0.04 m.sec-1*

Macroscopic analysis Figs. 6, 7 and 8. When the grinding speed was constant, the surface roughness increases with the increase of GF & GT. Comparing Figs. 6(a), 7(a) and 8(a), with the increased of grinding speed, the surface roughness decreased and the grinding surface become smoother.

Microscopic analysis of Figs. 6, 7 and 8. shown that when the grinding speed was 0.02 m.sec^{-1} and the grinding force in Z direction was 59 N, the surface roughness was 8.5 μm. When the grinding speed was 0.04 m.sec^{-1} and the grinding force in Z direction was 59 N, the surface roughness was 5 μm. According to Figs. 6(b), 7(b), and 8(b), when grinding speeds were 0.02 m.sec^{-1}, 0.03 m.sec^{-1}, and 0.04 m.sec^{-1}, and grinding temperatures were 360 °C, the surface roughnesswas 8.5 μm, 6.2 μm, and 5 μm, respectively. When the GF & GT vary slightly (e.g. Fig. 6(a) and (b)), the surface roughness will also change. It shows that GF & GT are very sensitive to surface roughness.

4.2 Discussion on the range of single particle GF & GT on surface roughness

Range, also known as Range, is used to express the number of variances in statistical data. Combined with the test results in Tab. 3 and using the range Eq. (15), the range analysis results of X/Y/Z grinding force, grinding temperature and surface roughness were formulated, as shown in Tab. 4.

$$\begin{cases} R_j = \max(k_1^{\,j}, k_2^{\,j}, k_3^{\,j}) - \min(k_1^{\,j}, k_2^{\,j}, k_3^{\,j}) \\ K_i^{\,j} = K_i^{\,j} \,/\, j \cdots \langle (i = 1,2,3); (j = 1,2,3,4,5,6,7,8,9) \end{cases} \tag{15}$$

In Eq. (15), i represents the number of levels, j represents the number of factors, and K_{ij} represents the sum of test results of the i level corresponding to the j-column factors.

Tab. 4 *Range results of grinding parameters on shape control (X/Y/Z grinding force, grinding temperature and surface roughness)*

Project	Range analysis term	Grinding speed(m.sec^{-1})	Grinding depth(μm)
Grinding force F_x	Range *R*	0.22	0.24
Grinding force F_y	Range *R*	4.19	30.92
Grinding force F_z	Range *R*	9.72	56.49
Grinding temperature	Range *R*	231.26	440.75
Ra	Range *R*	2.24	8.06

In Tab. 4, because there were 9 factors in grinding depth, 1 (1 μm), 5 (16 μm) and 9 (50 μm) were selected as range analysis data for convenience of analysis. By analyzing the range *R* in Tab.4, the grinding depth had the greatest influence on the grinding force in X/Y/Z direction. Combined with the analysis of machining coordinates in Fig. 2, compared with grinding speed, the influence of grinding depth on grinding force in Y and Z directions were much greater than that in X, which was 7.38 times and 5.81 times of grinding speed respectively. The grinding depth is considered to be extreme points (1 (1 μm) and 9 (50 μm)) at both ends, which was basically consistent with the previous analysis results. With the increase of grinding force, the grinding temperature will also increase. In Tab. 4, grinding depth has the greatest effect on surface roughness, which is 3.6 times of grinding speed.

4.3 Experimental analysis

Based on the above simulation analysis, the precision aerospace spindle bearing was machined and roughness inspection was carried out, as shown in Fig. 9. After passing the inspection, the bearing was tested at high speed for 225 hours, and the test results were shown in Fig. 10.

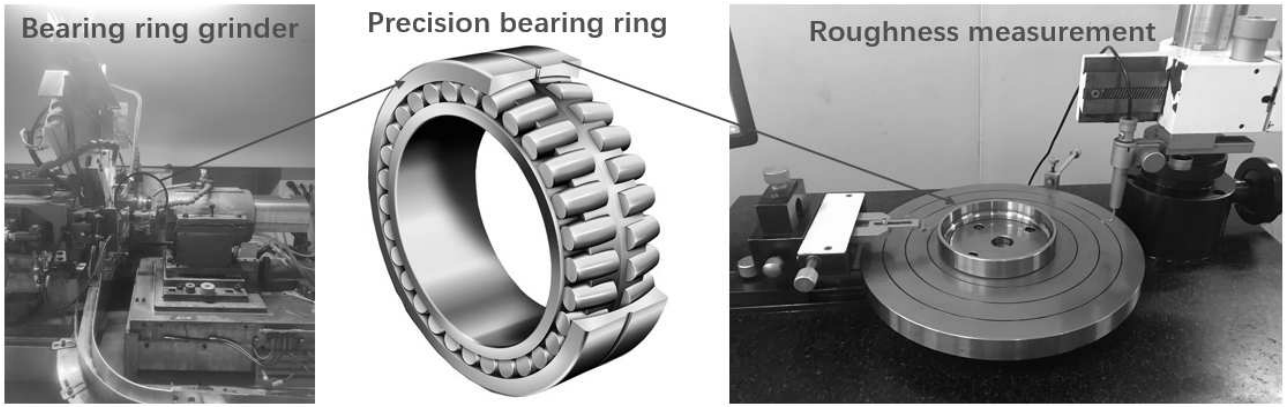

Fig. 9 *Machining and roughness inspection of precision aerospace spindle bearings*

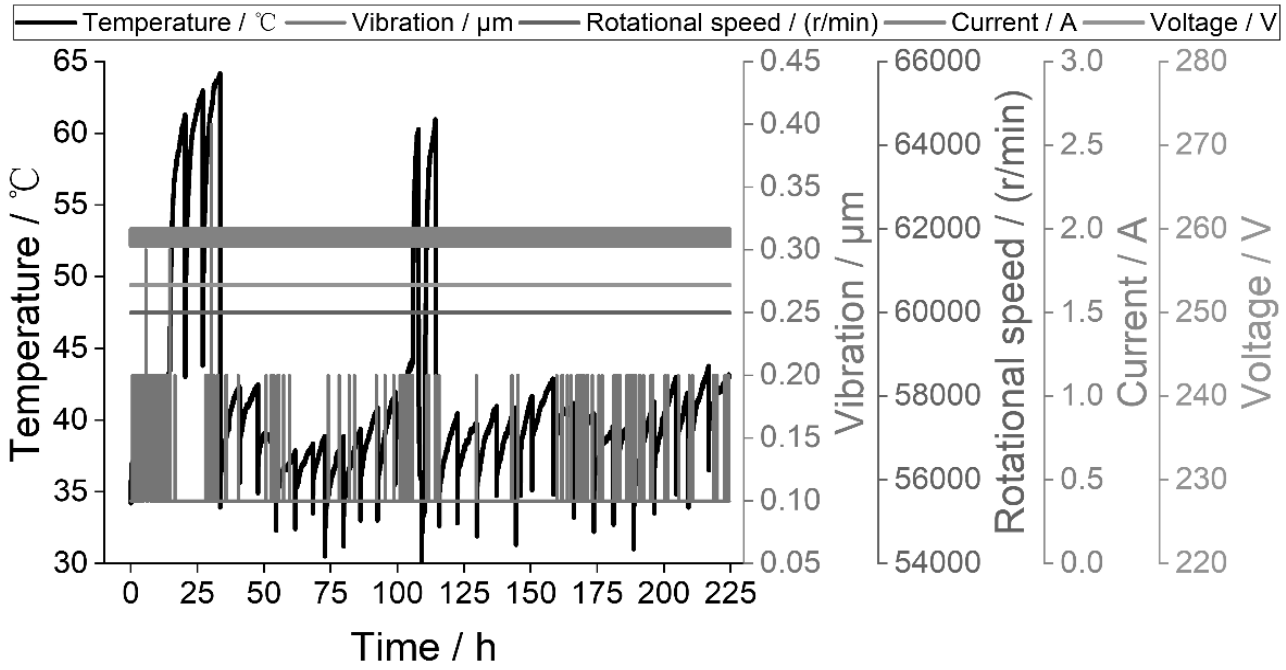

Fig. 10 *High-speed experiment of precision aerospace spindle bearing*

The purpose of bearing high speed experiment was to analyze whether the temperature, vibration, current and voltage of bearing outer ring meet the requirements under the continuous working condition of 60000 r/min, and to comprehensively analyzed the relationship between bearing outer ring temperature, vibration and voltage and rotational speed.

In Fig. 10, the bearing temperature was between 30 °C and 65 °C, and most of them were within 44 °C when the test speed was constant at 60000 r/min. Meanwhile, the vibration of the bearing was between 0.1 μm and 0.2 μm, the current was between 1.8 A – 2.0 A, and the voltage was constant at about 255 V. This data meets the requirements of bearings, and all indexes are controllable.

5 Conclusion

- The grinding force in Z direction was compressive stress, the grinding force in X direction was tensile stress, and the grinding force in Z direction was always greater than that in X and Y directions. The grinding force in X direction is always 0 N. With the increase of grinding depth, the GF & GT in X and Z directions gradually increase. However, the grinding temperature does not increase linearly with the increase of grinding depth, and at a certain moment, the grinding temperature will change differently.

- When the grinding speed was constant, the surface roughness increased with the increase of GF & GT. With the increase of grinding speed, the surface roughness decreases and the grinding surface is smoother. It accords with the actual working conditions and shows that GF & GT are very sensitive to the influence of surface roughness.
- Through range analysis, grinding depth had the greatest influence on grinding force in X/Y/Z direction. Compared with the grinding speed, the influence of grinding depth on the grinding force in Y and Z directions was much greater than that in X, which was 7.38 times and 5.81 times of the grinding speed, respectively. With the increase of grinding force, the grinding temperature will also increase. Grinding depth has the greatest influence on surface roughness, which was 3.6 times of grinding speed.
- When the rotating speed of precision aerospace bearing was constant at 60 000 $r.min^{-1}$, the bearing temperature was between 30 °C and 65 °C and most of them are within 44 °C. The test data meet the requirements of bearings, and all indexes were controllable. It indicates that the research in this study can provide reliable theoretical and experimental data support for related research fields.

Declaration of competing interest

The authors declare that they have no known competing financial interests or personal relationships that could have appeared to influence the work reported in this paper.

Funding

This research was funded by the National Key R&D Program of Manufacturing Basic Technology and Key Components (2023YFB2406400).

Acknowledgments

The authors wish to acknowledge Dr Chen, professor of Xi'an Jiaotong University, for his help in interpreting the significance of the results of this study.

Data availability

Data will be made available on request.

References

[1] BAKSA T, ADAMEK P, HRONEK O, ZETEK M. (2019). Degradation of a Grinding Wheel when Grinding Cermet Materials and Its Influence on the Grinding Process [J]. *Manufacturing Technology*. 19(1):9-13.

[2] BAKSA T, FARSKY J, HRONEK O, ZETEK M. (2018).Impact of Cutting Speed on Grinding Wheel Wear and Cutting Force when Grinding Cermet [J]. *Manufacturing Technology*. 18(5):699-703.

[3] LEI X , XIANG D , PENG P ,LIU G., LI B., ZHAO B., GAO G. (2022).Establishment of dynamic grinding force model for ultrasonic-assisted single abrasive high-speed grinding [J].*Journal of Materials Processing Technology*.

[4] ZHOU W , TANG J , SHAO W , WEN J. (2022).Towards understanding the ploughing friction mechanism in ultrasonic assisted grinding with single grain [J].*International Journal of Mechanical Sciences*. 222:107248.

[5] YAN S J, XU X H, YANG Z Y, ZHU D H, DING HAN. (2019). An improved robotic abrasive belt grinding force model considering the effects of cut-in and cut-off [J]. *Journal of Manufacturing Processes*. 37(JAN.):496-508.

[6] KRZYSZTOF N , SEWERYN K. (2020). New approach for cooling and lubrication in dry machining on the example of internal cylindrical grinding of bearing rings [J].*Sustainable Materials and Technologies*. 24(00166).

[7] HE C L, ZHANG J, GENG K. WANG S Q, LUO M J, ZHANG X N, REN C Z. (2022).Advances in ultra-precision machining of bearing rolling elements [J]. *The International Journal of Advanced Manufacturing Technology*. 122, 3493–3524.

[8] CAI S, YAO B, ZHENG Q, (2020). Dynamic grinding force model for carbide insert peripheral grinding based on grain element method [J]. *Journal of Manufacturing Processes*. 58(2020):1200-1210.

[9] TK B, KT B, TK A. (2020). Effect of grinding fluid supply on workpiece temperature in continuous generating grinding [J]. *Journal of Manufacturing Processes*. 60:410-417.

[10] YAO C F, WANG T, XIAO W, HUANG X C, REN J X. (2024). Experimental study on grinding force and grinding temperature of Aermet 100 steel in surface grinding [J].

Journal of Materials Processing Technology. 214(11): 2191-2199.

[11] GONG P, ZHANG Y, WANG C. (2023). Residual Stress Generation in Grinding: Mechanism and Modeling [J]. *Journal of Materials Processing Technology*. 118262.

[12] DING H, LI H P, SHAO W, TANG J Y. (2021). Prediction and control for local bearing contact-based collaborative grinding of non-orthogonal aerospace spiral bevel gears [J]. *Mechanical Systems and Signal Processing*. 160: 107841.

[13] QIN F, ZHANG L, CHEN P. (2021). In situ wireless measurement of grinding force in silicon wafer self-rotating grinding process [J]. *Mechanical Systems and Signal Processing*. 154:107550.

[14] HU L, CHEN Y. (2023). Surface integrity and fatigue life test of products under coupling grinding force and temperature [J]. *The International Journal of Advanced Manufacturing Technology*. 129(3), 1035-1052.

[15] BAKSA T, FARSKY J, HRONEK O, ZETEK M. (2018). Influence of Depth of Cut on Quality of Ground Surface and Cutting Force when Grinding Cermet [J]. *Manufacturing Technology*. 18(3):352-356.